JOURNAL OF MATERIALS SCIENCE 17 (1982) 359–368

Mechanical behaviour of an amorphous metal ribbon reinforced resin-matrix composite

J. R. STRIFE, K. M. PREWO
United Technologies Research Center, East Hartford, Connecticut 06108, USA

Resin-matrix composites, reinforced with high aspect ratio 2826MB amorphous metal ribbon in a simple stacking pattern, were fabricated and evaluated. Typical composite properties at 60 vol% ribbon are a density of 5.27 g cm^{-3}, a longitudinal tensile strength of 1740 MPa, a transverse tensile strength of 870 MPa, a near-isotropic in-plane modulus of 100 GPa and a fracture toughness similar to that of 6061-T6 aluminium alloy. These composites are also shown to have poor mechanical fatigue resistance. In comparison with other engineering materials, these composites are superior on a specific strength basis. However, they are not competitive with quasi-isotropic AS graphite–epoxy on a specific modulus basis. Because of this deficiency, it is concluded that amorphous metal ribbon reinforced composites would not be in a competitive position for most high performance composite applications. However, the high biaxial composite strength properties, potential low cost, and the unusual soft magnetic properties offered by the ribbons may result in some unique composite applications.

1. Introduction

The primary structural advantage offered by the use of ribbon materials as the reinforcing phase in composites is their ability to offer significant improvements in transverse composite properties while maintaining axial properties equivalent to fibre reinforced composites. The degree of isotropy of the in-plane mechanical properties of unidirectionally-reinforced ribbon composites is controlled by the ratio of ribbon width, w, to the ribbon thickness, t, the aspect ratio, w/t. If this ratio is sufficiently high, virtually isotropic properties are achieved. In contrast, in-plane isotropy in fibre reinforced systems is achieved through multi-directional lay-up patterns such as $[0, \pm 45°, 90°]_n$. Thus, although a similar degree of isotropy may be achieved in a fibre reinforced composite, it is achieved at a significant loss in axial properties.

In spite of the structural advantage offered by the use of ribbons as reinforcement, several factors have impeded their use. The primary problem has been the lack of a low cost process to consistently produce high performance ribbon material. The optimum performance on a specific property basis is offered by ceramic reinforcements such as boron and silicon carbide or glass reinforcements. These materials, however, exhibit the classic "size-effect" problem, characteristic of brittle materials, so that wide ribbons cannot be consistently produced at reasonable cost having the same strength or strength variation as the fibre form.

Because of the "size-effect" problem associated with ceramics and oxide glasses, several investigators turned to the use of metals such as steel and aluminium in ribbon form as the reinforcement in resin matrices [1–4]. Rule-of-mixture axial strength and modulus were achieved simultaneously with excellent transverse properties. Transverse to axial composite ratios, σ_{90}/σ_0, in excess of 0.60 and modulus ratios, E_{90}/E_0, in excess of 0.9 were measured. These same ratios are generally less than 0.1 in fibre reinforced systems.

The discovery of amorphous metal alloys and their ability to be continuously cast has presented the composite scientist with a unique reinforcement which offers several advantages with respect to other metallic reinforcements. Amorphous metals have specific strengths significantly higher than those offered by cold-rolled steel alloys. The cold-rolled steels have an upper limit on

0022–2461/82/020359–10$3.00/0

specific strength of approximately 31.3×10^3 m while iron-base amorphous metal alloys have exhibited specific strengths of 49.9×10^3 m. In spite of their very high strength and amorphous structure, amorphous metal alloys do not exhibit the "size-effect" characteristic of ceramics and glasses. In ribbon form, these materials are easily handled and can actually be crimped before failure occurs. Other possible advantages depending on composition are excellent corrosion resistance and unusual magnetic softness. Finally, fabrication of amorphous metal ribbon is in principle a low-cost forming process since the shaping process is opposed by shear resistance of a liquid rather than a solid, as in drawing or rolling operations.

In a previous investigation by the present authors [5] composite parameters were investigated using high-strength Metglas* alloy 2826MB ribbon material as the reinforcement with an epoxy–nylon adhesive, FM-1000 as the matrix. The effects of ribbon aspect ratio and ribbon stacking pattern on transverse composite properties were determined and rationalized using the concept of critical transfer length. In this paper, the results of an assessment of composite mechanical properties are presented for 2826MB–FM-1000 composites constructed with high aspect ratio ribbon in a simple stacking pattern.

2. Materials and composite fabrication

2.1. Materials

An amorphous metal ribbon having a nominal composition of $Fe_{40}Ni_{38}Mo_4B_{18}$ and designated Metglas alloy 2826MB was selected as the ribbon material for the programme since it possessed the best mechanical properties of the high aspect ratio ribbon materials commercially available. Approximately 4 kg of 2826MB ribbon, nominally of 13 mm width, were purchased from Allied Chemical Corporation for the test programme. The ribbon was cast continuously in one production run by the vendor.

Based on the results of the previously reported study [5], FM-1000 adhesive film supplied by Americal Cyanamid was selected as the matrix material. A minimum film weight of $0.073\ kg\ m^{-2}$ was selected since this allowed high ribbon volume per cent composites to be fabricated without excessive resin flow.

2.2. Composite fabrication

A precursor tape 150 mm in width was fabricated by winding the ribbon over the adhesive on a spring-loaded mandrel. A heated iron was then passed over the ribbon surfaces at a slow rate. Due to the thermoplastic nature of the film, a controlled amount of heating served to initiate bonding without causing any extensive curing. This procedure served to imbed the ribbon in the film resulting in a precursor tape exhibiting excellent handling properties. Ribbon spacing was controlled to approximately 0.5 mm.

Plies of the proper dimension were cut from the tape material and laid up in steel dies using a simple stacking pattern where one half of the ribbon width was overlapped from layer to layer, see Fig. 1. The composites were then hot-pressed in air by initially applying 1.38 MPa pressure at 163° C, and maintaining this pressure for 1 h at 177° C. Ribbon volume percentages of 60 were typically achieved using these parameters. The composite density at this ribbon volume per cent was $5.27\ g\ cm^{-3}$.

3. Test procedures

3.1. Tensile testing at room temperature

The composite tensile properties were characterized with ribbons oriented both parallel with and transverse to the specimen tensile axis. Eight layer composite panels of dimensions 76 mm × 152 mm were fabricated according to the schedule outlined previously. Ribbon volume percentages were determined from density measurements assuming no porosity and using a density of $8.02\ g\ cm^{-3}$ for the 2826MB ribbon and $1.15\ g\ cm^{-3}$ for the FM-1000 matrix. Tensile specimens 6.35 mm in width were cut from the panels, and fibreglass doublers were bonded to the speci-

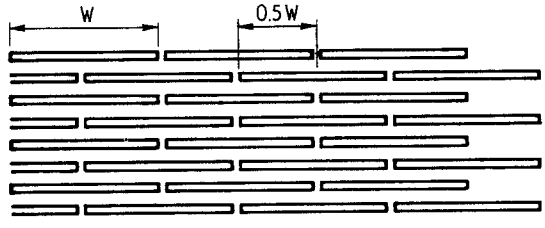

Figure 1 Schematic transverse cross-section of ribbon lay-up pattern used in composite fabrication.

* Metglas is a trademark of Allied Chemical Corporation.

mens providing a gauge section of 50 mm. Resistance strain gauges were bonded to both sides of the specimens for determination of the elastic modulus and failure strain. Tensile testing was performed at a constant cross-head speed of 0.25 mm min^{-1}.

3.2. Tensile testing after environmental exposure

The composite transverse tensile strength was determined after exposure to specific environmental conditions. In particular, since the resin was an epoxy–nylon, exposure to elevated temperature or moisture were anticipated to have a deleterious effect on the composite transverse tensile strength.

Review of available vendor data indicated that a maximum exposure temperature of 82° C was appropriate for the resin system utilized. The effect of elevated temperature on composite transverse tensile strength was evaluated by testing transverse tensile specimens prepared from eight ply panels, as described in Section 3.1, at 82° C in air atmosphere. To determine the effect of thermal fatigue on composite transverse tensile strength, as-fabricated composite panels were cycled between room temperature and 82° C a total of 500 times. Single cycle time was 20 min with 5 min exposure at the temperature limits. After this thermal cycling, transverse tensile specimens were prepared as described in Section 3.1 and tension tested at room temperature.

The effect of moist environment on composite transverse tensile strength was determined by exposing transverse tensile specimens to 95% relative humidity at 60° C for 21 h. Weight-gain measurements indicated that saturation occured in less than 4 h under these conditions. On removing specimens from the humidity chamber, it was noted that small irregular patches of rust had formed on the outer ply ribbon surfaces. Subsequent tensile testing was performed at room temperature.

3.3. Fatigue testing at room temperature

Composite tensile specimens were prepared from eight ply panels, as described in Section 3.1 for testing in tension–tension fatigue. All specimens were tested at a minimum to maximum stress ratio of 0.1. Tests were terminated either after failure or accumulation of 10^6 fatigue cycles.

3.4. Impact resistance and fracture toughness at room temperature

Composite impact resistance and fracture thoughness were assessed using the instrumented pendulum impact test. The test apparatus consisted of a standard 31.2 J capacity pendulum impact machine equipped with an instrumented tup (input device) which permitted the generation of load–time traces describing the impact event. Continuous load measurements were achieved through the use of strain gauges mounted on the tup and a calibration to translate strain into load. The strain-gauge output was monitored on an oscilloscope producing a load–time trace which was then photographically recorded.

The composite specimens tested were all of non-standard width and depth. However, all the specimens were notched in accordance with the specifications of ASTM standard E-23 [6], for testing of sub-size Charpy specimens. To insure uniform impact loading for specimens of different depth, shims were fabricated to position the specimen impact face properly with respect to the bottom of the pendulum swing.

Composite specimens tested with ribbons oriented both parallel with and transverse to the specimen long axis are referred to as the longitudinal and transverse orientations, respectively. The specimen dimensions were nominally 40 mm × 6.35 m × d, where d is the overall unnotched beam width in mm. For the longitudinal orientation, laminates were constructed having beam depths of 1.59, 3.18 and 6.35 mm. For the transverse orientation, all specimens had an unnotched depth of 1.59 mm. In both the longitudinal and transverse orientations, the specimens were oriented such that they were struck normal to the plys, not on the ply edges. A tup velocity of 1.06 m sec^{-1} was used to eliminate the impulse peak from the load–time traces.

4. Ribbon properties

Throughout the process of composite fabrication, ribbon samples were removed to continually monitor the ribbon tensile strength and ribbon dimensional characteristics. The cross-sectional areas, determined by weight measurement assuming a ribbon density of 8.02 g cm^{-3}, varied by approximately 2% around a mean value of 2.24 × 10^{-2} mm^2. The ribbon width was constant at 13.2 mm, and the average ribbon thickness was 0.043 mm. The ribbon aspect ratio, w/t, was there-

fore 308. Ribbon cross-sections were examined metallographically and found to be very uniform. Ten groups of five ribbon samples were tensile tested to monitor ribbon strength. The average ribbon strength was 2570 MPa with a coefficient of variation of 0.15. The ribbon elastic modulus is quoted to be 165 GPa by the manufacturer and was determined as 159 GPa using extensional wave-velocity measurements and 165 GPa from plots of ribbon tensile specimen compliance as a function of gauge length.

5. Composite properties

5.1. Tensile properties

The longitudinal elastic modulus, E_0, and tensile strength, σ_0, determined as a function of ribbon volume-fraction are plotted in Figs 2 and 3, respectively. Lines representing the rule-of-mixtures corresponding to a ribbon tensile strength of 2570 MPa and ribbon modulus of 165 GPa are included for comparison purposes. The matrix contribution was assumed to be zero. It is evident from Fig. 2 that the measured composite modulus is closely approximated by the rule-of-mixtures prediction. However, it is evident in Fig. 3 that the composite strengths are significantly greater than that predicted by the rule-of-mixtures using a ribbon tensile strength of 2570 MPa. The data can be more closely approximated assuming a ribbon tensile strength of 2900 MPa. Typical longitudinal stress–strain curves are shown in Fig. 4. The stress–strain behaviour was linear elastic to a strain level of approximately 0.01; beyond this point a slightly decreased modulus was observed until failure. Failure strains varied between 0.017 and 0.020. Tensile fractures were flat and occured at 90° to the tensile axis.

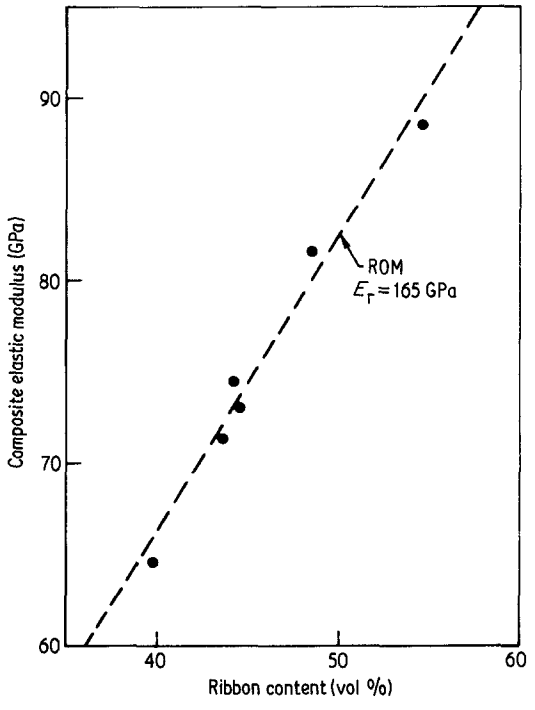

Figure 2 Axial composite elastic modulus as a function of ribbon content.

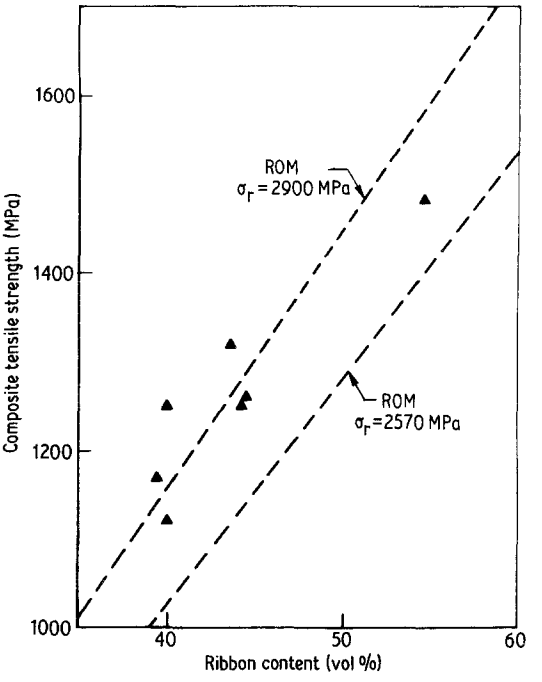

Figure 3 Axial composite tensile strength as a function of ribbon content.

The transverse tensile stress–strain behaviour was determined using specimens cut from a panel having an average of 58 vol% ribbon. The average transverse tensile strength, σ_{90}, was 806 MPa, the average transverse tensile modulus, E_{90}, was 112 GPa, and the average failure strain was 0.0068. Assuming an average ribbon strength of 2900 MPa, σ_0 can be calculated at this ribbon volume-fraction, given a composite strength ratio, σ_{90}/σ_0, of 0.48 This value is in close agreement with the strength of 0.50 predicted for this stacking pattern [5]. Note that in the simple stacking pattern, Fig. 1, the anticipated fracture path is along the plane of weakness defined by the ribbon gaps. Along this fracture path, the fraction of ribbons broken is 0.50 and there is no pull-out contribution from the other layers. Thus, the strength ratio, σ_{90}/σ_0,

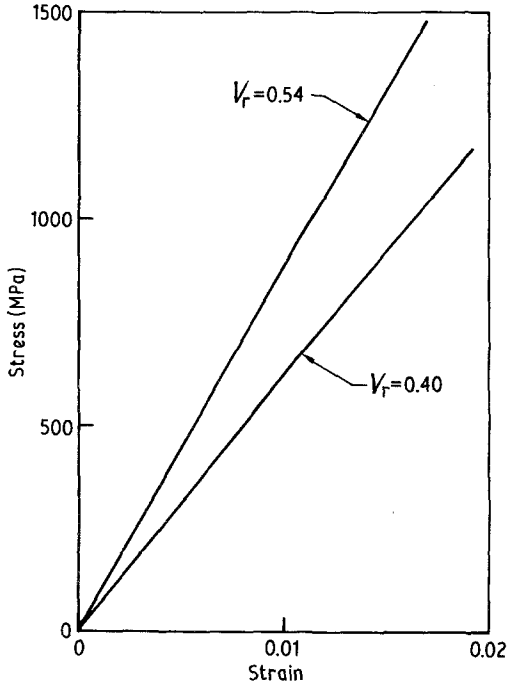

Figure 4 Axial tensile stress–strain behaviour at room temperature for composites containing ribbon volume percentages of 40% and 54%.

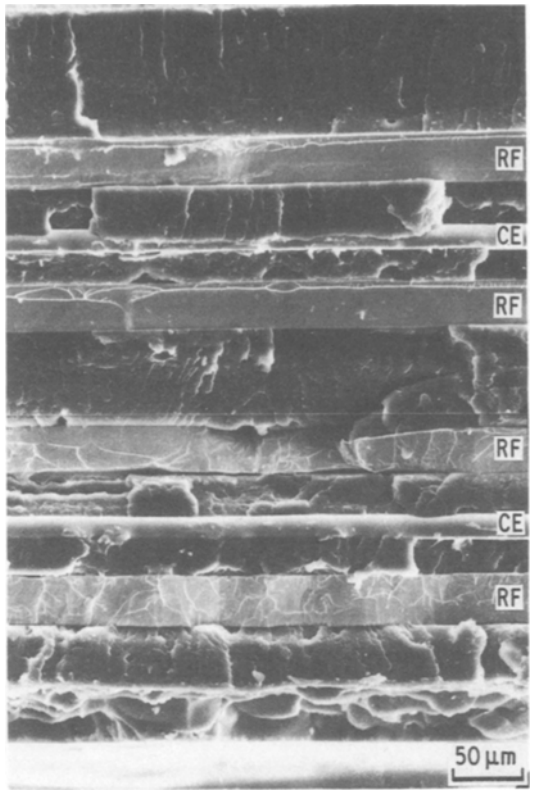

Figure 5 Fracture surface of transverse tensile specimen, where RF denotes ribbon fracture and CE denotes the locations of ribbon cast edges debonded from the resin matrix.

is predicted as 0.50. Observation of transverse composite fracture surface in the scanning electron microscope (SEM), Fig. 5, confirmed the anticipated fracture mode. As expected for an eight-layer composite, four ribbon fractures are observed. The cast ribbon edges of two intermediate layers are also visible in the SEM observations.

The transverse elastic properties of ribbon reinforced composites are primarily controlled by the ribbon aspect ratio. With the ribbon used in this investigation, an in-plane modulus ratio, E_{90}/E_0, of 0.94 is predicted from the Halpin–Tsai relations [7]. At a ribbon volume per cent, V_r of 58, the axial composite modulus is predicted to be 96 GPa. Thus, the anticipated transverse composite modulus is 90 GPa. As stated previously, the transverse elastic modulus was measured as 112 GPa, a significantly higher value. Examination of the stress–strain curves showed that the elastic modulus of these specimens increased as the failure strain was approached. Further testing of specimens revealed that the transverse stress–strain behaviour, as determined using strain gauges, was dependent on the location of the gauges on the specimen surface. Typical stress–strain behaviour for the two strain-gauge pair locations is shown in Fig. 6. When neither strain gauge over-

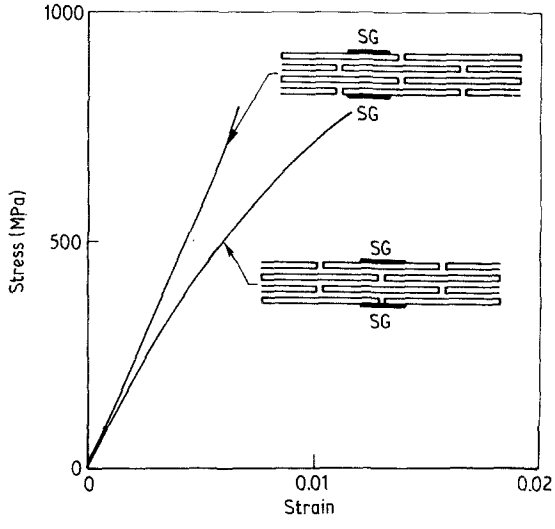

Figure 6 Composite transverse tensile stress–strain behaviour at room temperature. The locations of the strain gauge (SG) pairs on each test specimen are schematically indicated.

layed a ribbon gap, as in the data reported, the initial elastic modulus was higher than predicted and the apparent elastic modulus increased as the failure load was approached. When one gauge overlayed a ribbon gap, the initial elastic modulus was lower than predicted and was followed by an increase in strain as the load increased. It was concluded from these results that non-uniform deformation occurred along the length of the specimen when tested in transverse tension. Greater deformation occurred at the ribbon-gap locations, and this condition was aggravated as the failure strain was approached.

5.2. Effect of environmental exposure on transverse tensile properties

Also of interest in this resin-matrix system were the effects of elevated temperature, thermal fatigue, and exposure to moist environment on the transverse tensile strength, the results of these tests are summarized in Table I. Also included are the ribbon volume percentages determined from density measurements and the predicted room-temperature composite strength for the stacking pattern utilized.

As shown in Table I, the transverse strength determined at 82° C was reduced to 55% of the room-temperature value. This reduction in tensile strength was correlated with a change in specimen fracture mode. Ribbon pull-out, as well as ribbon fracture, occurred at 82° C. For the eight-layer composite tested, typical fracture surfaces exhibited two ribbons pulled out and two ribbons fractured. These results indicate that the ribbon–matrix bond strength was decreased at 82° C to the extent that the critical ribbon overlap required to prevent pull-out was greater than that provided by this ribbon width.

Although the composite transverse tensile strength was significantly reduced at 82° C with respect to room temperature, thermal cycling between room temperature and 82° C had no measurable effect on post-cycling room-temperature composite transverse tensile strength. It can be seen in Table I that the average tensile strength measured was very close to the predicted as-fabricated strength and unaffected by the thermal fatigue cycle utilized.

Finally, it is evident in Table I that exposure to a moist environment severely degraded the composite tensile strength. All specimens failed by ribbon pull-out indicating that the ribbon–matrix bond strength was severely degraded. Corrosion products were also evident along the edges of the interior ply ribbons but to much lesser extent than observed on the outer ply ribbon surfaces. These factors point to the need for corrosion-resistant ribbon compositions and composite protective coatings.

5.3. Mechanical fatigue properties

The tension–tension fatigue behaviours of composites with ribbons both oriented parallel with and transverse to the stress axis were determined. In order to compare the data obtained, the ratio of the maximum applied fatigue stress, σ_{max}, to the calculated composite tensile strength, σ_c, σ_{max}/σ_c, was plotted as a function of cycles-to-failure. These data are presented in Fig. 7 for both longitudinal and transverse ribbon orientations.

Two groups of specimens were tested with ribbons in the longitudinal orientation. In the first group, specimens were cut from panels constructed with the 0.5 W overlap pattern as in Fig. 1. As shown in Fig. 7, a 10^6 cycle fatigue life was achieved using these specimens at a maximum stress to composite strength ratio, σ_{max}/σ_c of 0.11. This is very low when compared with fibre reinforced resin matrix composite systems such as As-graphite–epoxy, where this ratio is typically in the range of 0.6 to 0.7. It was thought that this poor fatigue resistance of longitudinal samples might be attributed to the specimen cutting operation. If the ribbon were notch senstive, then

TABLE I Composite transverse tensile strength

Exposure	Test temperature (°C)	Ribbon content, V_r (vol %)	Transverse tensile strength	
			Measured (MPa)	Predicted* (MPa)
as-fabricated	20	58	806	841
as-fabricated	82	58	449	841
thermal cycling	20	64	913	928
95% relative humidity 60° C	20	64	150	928

* $\sigma_{90} = 0.5\ \sigma_r V_r$ for as-fabricated specimens tested at 20° C.

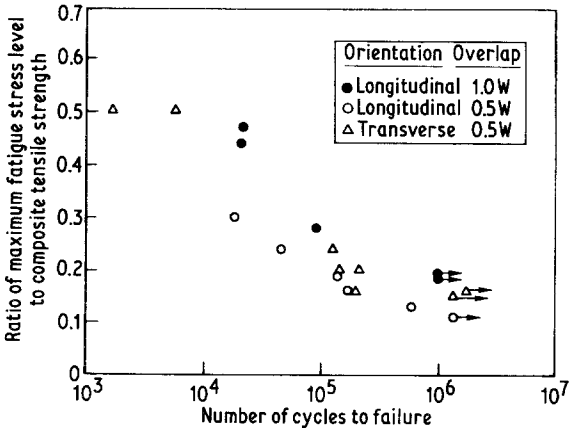

Figure 7 Composite tension–tension fatigue behaviour (R = 0.1).

defects induced along the specimen length in those areas where ribbons were cut during specimen preparation could reduce fatigue strength. To assess this possibility, a second group of composite specimens was fabricated such that the as-received ribbon edges were preserved. This was accomplished by fabricating single-ribbon width eight-layer composite laminates, i.e., with an overlap of 1.0 *W*. As before, the specimens were tested using a stress ratio of 0.1. The data for these specimens, also included in Fig. 7, indicate that the composite laminates fabricated using uncut ribbons have better fatigue resistance than specimens cut from a composite panel. A 10^6 cycle fatigue life was achieved for a maximum stress to composite strength ratio of 0.19. Although this represents a considerable improvement in fatigue life, longitudinal composite fatigue performance is still low.

With ribbons oriented at 90° to the tensile axis, the composite fatigue resistance is similar to that observed with ribbons oriented at 0° to the tensile axis, Fig. 7. A 10^6 cycle fatigue limit was achieved for a maximum stress-to-composite strength ratio, σ_{max}/σ_c, of 0.16. This ratio is greater than that observed for the longitudinal specimens cut from panels but is less than that observed for the uncut longitudinal laminates.

In summary, these data indicate that for 60 vol% ribbon with a simple overlap pattern the approximate 10^6 cycle fatigue limits are 330 MPa for the longitudinal ribbon orientation and 140 MPa with ribbons oriented transversely. These values are less than 20% of the composite static strength. In comparison with fibre reinforced composites, the fatigue resistance of these amorphous metal ribbon reinforced composites is low.

Observation of fatigued samples showed that the macroscopic failure mode of the composites was identical to composites failed in static tension. No extensive delamination or other damage was observed as a function of fatigue loading. This observation suggested that the fatigue resistance of the amorphous metal ribbon was low relative to its tensile strength.

5.4. Impact resistance and fracture toughness

A summary of the specimens tested in the instrumented pendulum impact apparatus and the data recorded is presented in Table II. A typical load–time trace obtained is shown in Fig. 8. Interpretation of the impact response of composites is generally complicated since it often depends on specimen geometry and the resultant imposed stress state. It is well known from beam theory that the failure mode in three-point bending is dependent on the test span-to-depth ratio. In general, for high longitudinal strength composites, tensile failures are observed at large span-to-depth ratios. Thus, the impact energy measured can depend to a large extent on the test span-to-depth ratio. To assess the relative role of these phenomena in the test results reported, the maximum flexural stress at failure was calculated using the equation

TABLE II Results of instrumented impact testing

Orientation	V_r (vol%)	Specimen width (mm)	Overall specimen depth (mm)	Maximum load (N)	Impact energy (J)
Longitudinal	60	6.86	1.58	267	0.65
Longitudinal	60	6.91	1.58	236	0.65
Longitudinal	59	6.93	3.18	872	1.50
Longitudinal	58	7.06	3.18	805	1.49
Longitudinal	56	7.32	6.35	2680	3.10
Transverse	60	6.25	1.59	142	0.47
Transverse	60	6.27	1.59	125	0.49
Transverse	60	6.15	1.59	133	0.34
Transverse	60	6.25	1.59	182	0.50

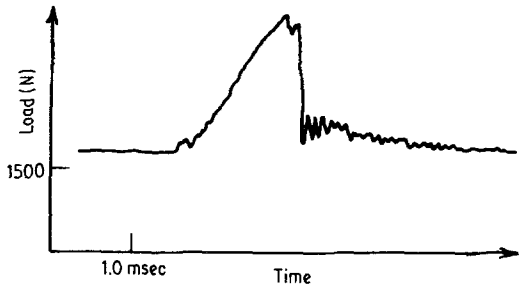

Figure 8 Instrumented impact trace for the longitudinal orientation and a net section depth of 5.03 mm.

$$\sigma_{max} = 3/2\ (PS/bd^2), \qquad (1)$$

where P is the load at failure, S is the span, b is the beam width, and d is the beam depth. In this case, the overall beam depth minus the notch was utilized for d.

For the longitudinally reinforced composites, the values of maximum flexural stress at failure are compared with the energy per unit area dissipated in Table III. It is evident that the test span-to-depth ratio, S/d, has a strong influence on the flexural stress at failure. As S/d decreased from 31.5 to 8.0, the flexural stress at failure decreased from 1450 MPa to 869 MPa indicating a probable contribution of shear failure at low S/d in the composites. In contrast to this indicated change in the stress-state at failure as a function of test geometry, the energy dissipated per net section area was not strongly affected. The energy per unit area increased by approximately 15% over the same range of S/d. This result was consistent with the observation that all specimens exhibited tensile failure of ribbons in the plane of impact with very little interlaminar failure. Thus, the above noted change in calculated flexural stress at failure was not explained.

Fig. 9 shows a comparison of the effect of test geometry on the notched bend specimen impact energy of this longitudinally reinforced composite and unreinforced metals tested similarly [8]. The

TABLE III Effect of test span-to-depth ratio on energy per unit area dissipated for longitudinal specimens

V_f (vol %)	Test span-to-depth ratio, S/d	Maximum flexural stress (MPa)	Energy per unit area (J m^{-2})
60	31.5	1450	74700
60	31.5	1270	74200
59	15.8	1170	85400
58	15.8	1060	83100
56	8.0	869	84400

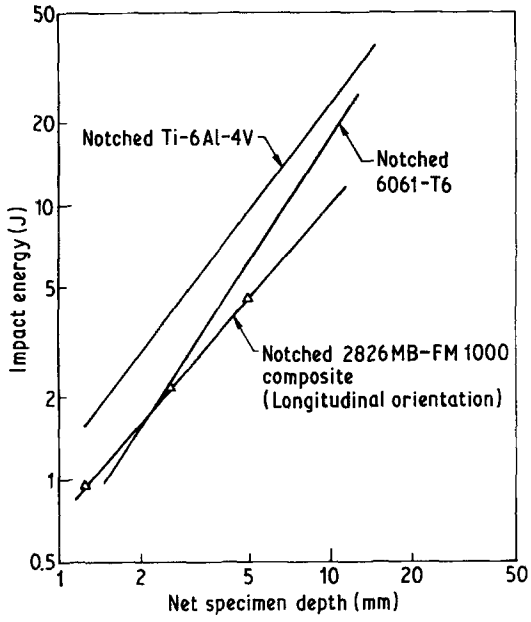

Figure 9 Energy dissipated as a function of specimen geometry for notched three-point bend impact specimens.

data for the composite specimens were normalized to the same specimen width as the metals assuming a linear dependence of impact energy on specimen width. Both the notched unreinforced metals and composite specimens exhibited a similar dependence of energy dissipated on net specimen depth. However, the composite dissipates equivalent impact energy only at the smaller net specimen depths tested.

With the ribbons oriented transversely, all specimens were tested at $S/d = 31.5$ and an average flexural strength of 869 MPa was measured. This correlates well with a calculated tensile strength of 869 MPa for the composite based on a ribbon strength of 2900 MPa. The average energy per unit area dissipated for the transverse specimen was 56900 J m^{-2} compared to 74500 J m^{-2} for longitudinal specimens of the same test geometry, i.e., $S/d = 31.5$. Observation of the fracture surfaces of the transverse specimens indicated a more irregular fracture plane in comparison with the longitudinal specimens. This was caused by a certain degree of ribbon sliding during fabrication which forced the crack to deviate significantly about the plane of weakness. This factor no doubt contributed to the energy measured for the transverse specimens. Thus, an even greater difference in energy dissipated between the two orientations would be expected for a perfect transverse lay-up.

TABLE IV Calculated K_{ID} values for Charpy V-notched specimens

Material	Orientation	K_{ID} (MPa m$^{-1/2}$)
2826MB–FM-1000*	Longitudinal	32.7 ± 8.0
	Transverse	17.5 ± 3.0
6061-T6	–	33.9
Ti-6A1-4V	–	135

* $V_r = 60$ vol %.

Finally, as a measure of resistance to crack growth, dynamic fracture thoughness values, K_{ID}, were calculated using the maximum load for fracture of the composite specimens. These data are listed in Table IV, together with values determined in a similar manner for Charpy V-notch specimens of Ti-6Al-4V and 6061-T6 in a previous investigation [8]. The longitudinally reinforced composites exhibit a fracture toughness, K_{ID}, similar to that observed for 6061-T6 aluminium alloy. With ribbons in the transverse orientation, the fracture toughness is half that of the longitudinal orientation.

6. Summary and conclusions

The results of this investigation have demonstrated that amorphous metal ribbon properties can be effectively translated into a resin–matrix composite. The utility of the ribbon format was demonstrated through the achievement of high values of composite axial and transverse tensile strength and elastic modulus. The strength and modulus properties could be readily predicted using relatively simple models coupled with existing theories. Several composite performance deficiencies were also identified and directly related to the 2826MB amorphous metal ribbon or the resin matrix. These included poor moisture resistance and poor composite fatigue properties.

A summary of the composite properties demonstrated in this investigation using a simple stacking pattern and a ribbon volume per cent of 60 is presented in Table V and compared with other selected engineering materials. Note that, for the graphite fibre-reinforced composite selected, the quasi-isotropic properties are used for comparison since the primary advantage offered by ribbon reinforcement is composite transverse to longitudinal property ratios which approach unity. On a specific strength basis, where the specific strength is the ratio of the strength, σ, to the density, ρ, the amorphous metal ribbon reinforced composite is competitive with the materials listed. In the longitudinal orientation, the specific strength is significantly greater than that of the other materials. Although this is not true in the transverse orientation for the composite listed, it may be anticipated that with alternate stacking patterns or further ribbon improvements, amorphous metal ribbon reinforced composite transverse strength equivalent to that offered by $[0, \pm 45°, 90°]_s$ AS graphite–epoxy can be achieved [9]. On a specific modulus basis, E/ρ, the amorphous metal ribbon reinforced composite is not competitive with $[0, \pm 45°, 90°]_s$ As graphite–epoxy having a specific modulus approximately 40% lower. This deficiency in specific modulus is one which cannot be overcome within the framework of existent amorphous metal ribbon technology. This is due to the fact that the elastic modulus to density ratio of most metallic materials is nearly invariant. Thus, improvements in ribbon modulus will be achieved con-

TABLE V Material property summary

Parameter*	Ribbon reinforced 2826MB–FM-1000†	AS-3501 $[0, \pm 45, 90]_s$ Graphite–epoxy	6061-T6 Aluminium alloy	Ti-6A1-4V
ρ (g cm^{-3})	5.27	1.58	2.72	4.43
σ_0 (MPa)	1740	450	310	1170
σ_{90} (MPa)	870	450		
E_0 (GPa)	99	48	69	114
E_{90} (GPa)	94	48		
ϵ_0 (%)	1.8	1.0	12	8.0
ϵ_{90} (%)	1.0	1.0		
Fatigue limit (MPa)	330 (0)	250 (0)	97	635
	140 (90)	250 (90)		
K_{ID} (MPa m$^{-1/2}$)	32.7 (0)	–	33.9	135
	17.5 (90)			

* 0 subscript refers to an axial measurement, 90 subscript refers to a transverse measurement.
† $V_r = 60$ vol %, simple overlap pattern.

currently with increase in density so that significant improvement in specific modulus properties is not foreseen. On comparing the other properties, it may be seen that the amorphous metal ribbon reinforced composite offers both advantages and disadvantages with respect to the other materials.

Because of the low specific modulus of amorphous metal ribbon reinforced composites, it is concluded that these composites will not be in a competitive position for most advanced composite applications, particularly in the aerospace industry, The advantages of the composite lie in the high biaxial strength properties, potential low cost, and perhaps in the unusual soft magnetic properties offered by the ribbons. Potential composite applications will therefore probably be limited to those which rely on the unique properties characteristic of this material.

Acknowledgement

This work was supported by the Air Force Wright Aeronautical Laboratories under Contract Number F33615-78-C-5063. The contract monitor was Mr George E. Husman, AFWAL/MLBC.

References

1. T. B. LEWIS, Proceedings of the 25th Annual Conference, Technical Society of the Plastics Industry, Section 8-D, (1970) p. 1.
2. L. A. GOETTLER, T. B. LEWIS and L. E. NIELSON, *Amer. Chem. Soc., Div. Polymer Chem.* **14** (1973) 436.
3. J. REXER, E. ANDERSON, G. FOURTY, C. BOURNAZEL and J. CORTEVILLE, Proceedings of the 1975 International Conference on Composite Materials Boston/Zurich (American Institute of Metallurgical Engineering) p. 758.
4. J. REXER and E. ANDERSON, *Polymer Eng. Sci.* **19** (1979) 1.
5. J. R. STRIFE and K. M. PREWO, *SAMPE J.* **10** (1980) 8.
6. 1979 Book of ASTM Standards, Part 10 (American Society for the Testing of Metals, Philadelphia 1979) p. 237.
7. J. E. ASHTON, J. C. HALPIN and P. H. PETIT, "Primer on Composite Materials: Analysis", (Technomic Publications, Stamford, CT, 1969).
8. K. M. PREWO, "Development of Impact Resistant Metal Matrix Composites", AFML-TR-75-216, March 1976.
9. J. R. STRIFE and K. M. PREWO, "Evaluation of Amorphous Ribbon Reinforced Resin Matrix Composites", AFWAL-TR-80-4060, April 1980.

Received 5 June
and accepted 29 June 1981